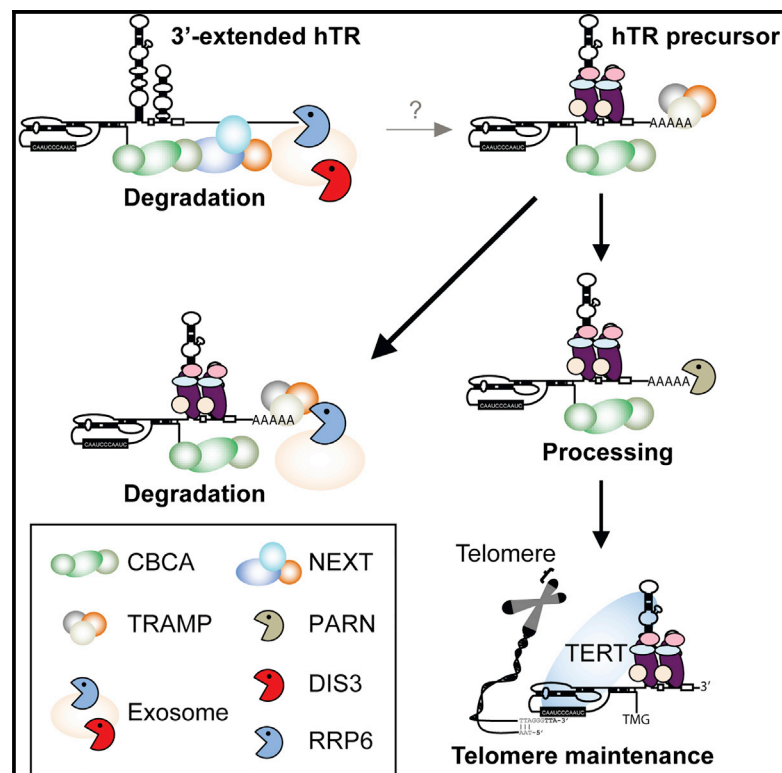


Human Telomerase RNA Processing and Quality Control

Graphical Abstract



Authors

Chi-Kang Tseng, Hui-Fang Wang, Allison M. Burns, Morgan R. Schroeder, Martina Gaspari, Peter Baumann

Correspondence

peb@stowers.org

In Brief

Tseng et. al. find that 3'-extended human telomerase RNA (hTR) is predominantly degraded by the exosome in concert with accessory factors. In contrast, shorter precursor hTR RNAs are oligo-adenylated by TRF4-2 and either processed by poly(A)-specific ribonuclease (PARN) or degraded by the exosome.

Highlights

- CBC/NEXT recruits the exosome to 3' extended forms of hTR
- Precursor hTR RNAs are oligo-adenylated by TRF4-2
- PARN competes with CBC/TRAMP/exosome-mediated degradation to generate mature hTR

Accession Numbers

GSE72055
GSE73776

Human Telomerase RNA Processing and Quality Control

Chi-Kang Tseng,^{1,2} Hui-Fang Wang,^{1,2} Allison M. Burns,² Morgan R. Schroeder,² Martina Gaspari,^{2,4} and Peter Baumann^{1,2,3,*}

¹Howard Hughes Medical Institute, Kansas City, MO 64110, USA

²Stowers Institute for Medical Research, Kansas City, MO 64110, USA

³Department of Molecular and Integrative Physiology, University of Kansas Medical Center, Kansas City, KS 66160, USA

⁴Present address: Dixie State University, School of Science and Technology, St. George, UT 84770, USA

*Correspondence: peb@stowers.org

<http://dx.doi.org/10.1016/j.celrep.2015.10.075>

This is an open access article under the CC BY-NC-ND license (<http://creativecommons.org/licenses/by-nc-nd/4.0/>).

SUMMARY

The non-coding RNA subunit of telomerase provides the template for telomerase activity. In diverse fungi, 3' end processing of telomerase RNA involves a single cleavage by the spliceosome. Here, we examine how human telomerase RNA (hTR) primary transcripts are processed into the mature form of precisely 451 nt. We find that the splicing inhibitor isoginkgetin mimics the effects of RNA exosome inhibition and causes accumulation of long hTR transcripts. Depletion of exosome components and accessory factors reveals functions for the cap binding complex (CBC) and the nuclear exosome targeting (NEXT) complex in hTR turnover. Whereas longer transcripts are predominantly degraded, shorter precursor RNAs are oligo-adenylated by TRF4-2 and either processed by poly(A)-specific ribonuclease (PARN) or degraded by the exosome. Our results reveal that hTR biogenesis involves a kinetic competition between RNA processing and degradation and suggest treatment options for telomerase insufficiency disorders.

INTRODUCTION

Telomerase is a ribonucleoprotein (RNP) complex, composed at its core of the catalytic protein subunit telomerase reverse transcriptase (TERT) and the RNA component telomerase RNA (TER). TERT repeatedly copies the template region of TER onto chromosome ends to replenish terminal DNA sequences lost during normal DNA replication (Nandakumar and Cech, 2013). The amount and activity of telomerase is tightly regulated in many higher organisms, and the absence of telomerase expression in most somatic cells is thought to function as a tumor-suppressive mechanism. Indeed, many cancers express high levels of telomerase, and their continued proliferation depends on telomerase activity (Stewart and Weinberg, 2006). Conversely, mutations in telomerase components cause a spectrum of degenerative syndromes including dyskeratosis congenita

(Mitchell et al., 1999b; Vulliamy et al., 2001), aplastic anemia (Vulliamy et al., 2002), and idiopathic pulmonary fibrosis (Armanios et al., 2007).

Although the catalytic protein component of telomerase is well conserved, the telomerase RNA subunit varies widely in length and sequence among species (Podlevsky et al., 2008). Consistent with the rapid evolution of the RNA, substantial differences have been noted in how the primary telomerase RNA transcripts are processed into the mature forms (Egan and Collins, 2012a). In the budding yeast *Saccharomyces cerevisiae*, transcriptional termination of TLC1 involves the Nrd1-Nab3-Sen1 (NNS) pathway (Jamonnak et al., 2011; Kuehner et al., 2011; Noël et al., 2012). The NNS complex interacts with TRAMP, a nuclear polyadenylation complex comprised of the poly(A) polymerases Trf4/5, the zinc-knuckle RNA-binding proteins Air1/2, and the RNA helicase Mtr4 (Tudek et al., 2014). TRAMP adds a short stretch of oligo-adenosine to the 3' ends of RNAs, which are then processed by the exosome, a multi-subunit complex with 3'-5' exonuclease activity (Coy et al., 2013; Houseley et al., 2006; Jamonnak et al., 2011; Kuehner et al., 2011; Lykke-Andersen et al., 2009; Mitchell, 2014).

In fission yeast, an intron downstream of the mature 3' end of TER1 is subject to the first cleavage reaction of splicing (Box et al., 2008). Instead of second cleavage and exon ligation, the 5' exon is released through a mechanism previously described to function in the discard of suboptimal splicing substrates (Kannan et al., 2013; Mayas et al., 2006). Spliceosomal cleavage appears to be widespread as a means of 3' end processing of telomerase RNA subunits in fungi with known examples in fission yeasts, *Aspergilli*, *Neurospora*, and *Candida* species (Gunisova et al., 2009; Kannan et al., 2015; Kuprys et al., 2013; Qi et al., 2015). Interestingly, conversion of splicing into a 3' end processing event has arisen multiple times independently, as examination of a handful of species revealed three distinct mechanisms for the uncoupling of the first and second transesterification reaction (Kannan et al., 2013, 2015; Qi et al., 2015).

Unlike yeast telomerase RNAs, which share similarities with small nuclear RNAs (Seto et al., 1999), vertebrate telomerase RNAs contain a box H/ACA motif (Mitchell et al., 1999a), a two-hairpin structure connected by a single-stranded hinge ANANNA (H box) and a 3' single-stranded tail containing the sequence ACA (Kiss et al., 2006, 2010). Most H/ACA box small

nucleolar RNAs (snoRNAs) and small Cajal-body-specific RNAs (scaRNAs) function as guides for site-specific pseudouridylation of rRNAs and small nuclear RNAs (snRNAs), respectively. However, no putative target of the human telomerase RNA (hTR) H/ACA motif has been identified, suggesting that the H/ACA motif in hTR may solely function to ensure processing and stability of the RNA. Consistent with the H/ACA domain being critical for hTR stability, several mutations in this region have been identified in patients with dyskeratosis congenita and cause defects in processing and localization of hTR (Fu and Collins, 2003; Theimer et al., 2007).

A key difference between mammalian telomerase RNAs and the vast majority of H/ACA snoRNAs is that the former are transcribed as independent units rather than being encoded within introns of other genes. Intron-encoded snoRNAs require splicing of the pre-mRNA to release a precursor that is debranched and processed by 5' to 3' and 3' to 5' exonucleases to generate the mature snoRNA (Kiss et al., 2006, 2010). hTR is transcribed from its own polymerase II (pol II) promoter and accumulates in the cell as an RNA of 451 nt in length. Longer forms have been reported (Feng et al., 1995; Theimer et al., 2007), but how primary transcripts are processed had remained elusive thus far (Figure S1).

RESULTS

Isoginkgetin Mimics the Effects of Inhibiting the RNA Exosome

Different means of generating the mature 3' end of telomerase RNA have been described in budding and fission yeasts (Figure S1). The spliceosome plays a direct role in the maturation of *S. pombe* TER1 (Box et al., 2008), and splicing is required for the release of intron-encoded H/ACA snoRNAs from pre-mRNAs (Kiss et al., 2006, 2010). Whether the spliceosome is also involved in the processing of hTR was not known. To examine the requirement of the spliceosome for hTR processing, we treated cells with isoginkgetin, a biflavonoid that inhibits spliceosomal splicing (O'Brien et al., 2008). Following exposure of cells for 12 hr, 3' extended forms of hTR increased by more than 20-fold, reminiscent of results in fungi and supporting a role for splicing in hTR processing (Figure 1A). No reduction in the mature form of hTR was observed upon isoginkgetin treatment (Figure S2A). This was not surprising, as half-lives between 7 and 32 days have been reported for hTR (Yi et al., 1999) and less than 10% of hTR would therefore be expected to turn over during the 12-hr exposure to isoginkgetin.

We next treated cells with spliceostatin A, another inhibitor of pre-mRNA splicing (Kaida et al., 2007). Examination of ~85,000 splicing units from Illumina RNA sequencing data revealed substantive global inhibition of splicing upon treatment with spliceostatin A, but only a modest reduction for isoginkgetin (Figure 1B). Nevertheless, unlike the effect observed with isoginkgetin, spliceostatin A treatment did not result in an increase in 3' extended forms of hTR (Figure 1C, right panel). Furthermore, several mutations of putative 5' splice sites downstream of position 451 failed to result in the accumulation of longer forms (data not shown). Similarly, replacing 500 bp of downstream sequence with unrelated DNA did not cause a reduction in mature hTR (Fu

and Collins, 2003). These observations were at odds with the hypothesis that the spliceosome is directly involved in hTR processing.

In examining differences in the effects of the two splicing inhibitors, we noticed that antisense reads upstream of the hTR locus increased specifically upon treatment with isoginkgetin (Figure 1C, left panel). Such promoter upstream transcripts (PROMPTs) have previously been observed to increase upon depletion of the RNA exosome (Preker et al., 2008). Further supporting the notion that isoginkgetin treatment mimics effects of reduced exosome activity, 3' extended transcripts at RNU1-1 and replication-dependent histone loci (Andersen et al., 2013) also increased in isoginkgetin-treated, but not spliceostatin A-treated, cells (Figure S2B).

Longer Forms of hTR Are Preferentially Degraded

The RNA exosome supplies the major 3' to 5' exonuclease activity in the cell and is responsible for the processing and elimination of many RNA species (Mitchell, 2014). To examine whether the exosome is involved in hTR biogenesis, we depleted the core exosome component RRP40 and the two exosome-associated nucleases RRP6 and DIS3, respectively (Figure 2A). Knockdown of RRP40 resulted in co-depletion of RRP6 (Figure 2A, lane 2) and caused a 13-fold increase in hTR forms extending by at least 50 nt beyond the mature 3' end (Figure 2B). Increases in 3' extended forms were also observed in the RRP6/DIS3 double and individual knockdowns, with RRP6 knockdown having a greater effect than DIS3 knockdown (Figure 2B). High-throughput sequencing of ribo-depleted RNA from knockdown samples confirmed increased read density downstream of the mature 3' end of hTR, as well as an increase in hTR PROMPT reads, in particular for the RRP40 depletion (Figure 2C). This accumulation of 3' extended forms of hTR in exosome-depleted cells supports the notion that the exosome either processes 3' extended forms into mature hTR or is responsible for their degradation.

To assess whether longer forms are preferentially degraded or processed, we cloned the hTR H/ACA box (nucleotides 206–451) and placed this 246-nt double-hairpin (DH) structure either 50 or 250 nt downstream of position 451 (Figure S3, shown in red). If 3' extended forms of ~750 nt or more normally give rise to the mature form via exonucleolytic trimming, processing will now be attenuated at the second H/ACA box placed downstream and a longer product will be formed at the expense of the 451-nt RNA. If, however, longer transcripts are normally degraded, then the same amount of 451-nt RNA will be produced in the presence and absence of the downstream H/ACA box. The longer forms, which are normally degraded, may give rise to an additional stable product visible in the form of a slower migrating band only if transcription extends beyond the 3' end of the newly introduced H/ACA box. Expression of the double H/ACA box constructs and wild-type hTR control in VA13 cells revealed similar amounts of 451-nt RNA (Figure 2D). Each of the double H/ACA box constructs produced an additional band of the expected size with substantially more product observed when the second H/ACA box was placed closer to position 451. These results indicate that long transcripts are predominantly degraded and that most transcripts are shorter than 1,000 nt.

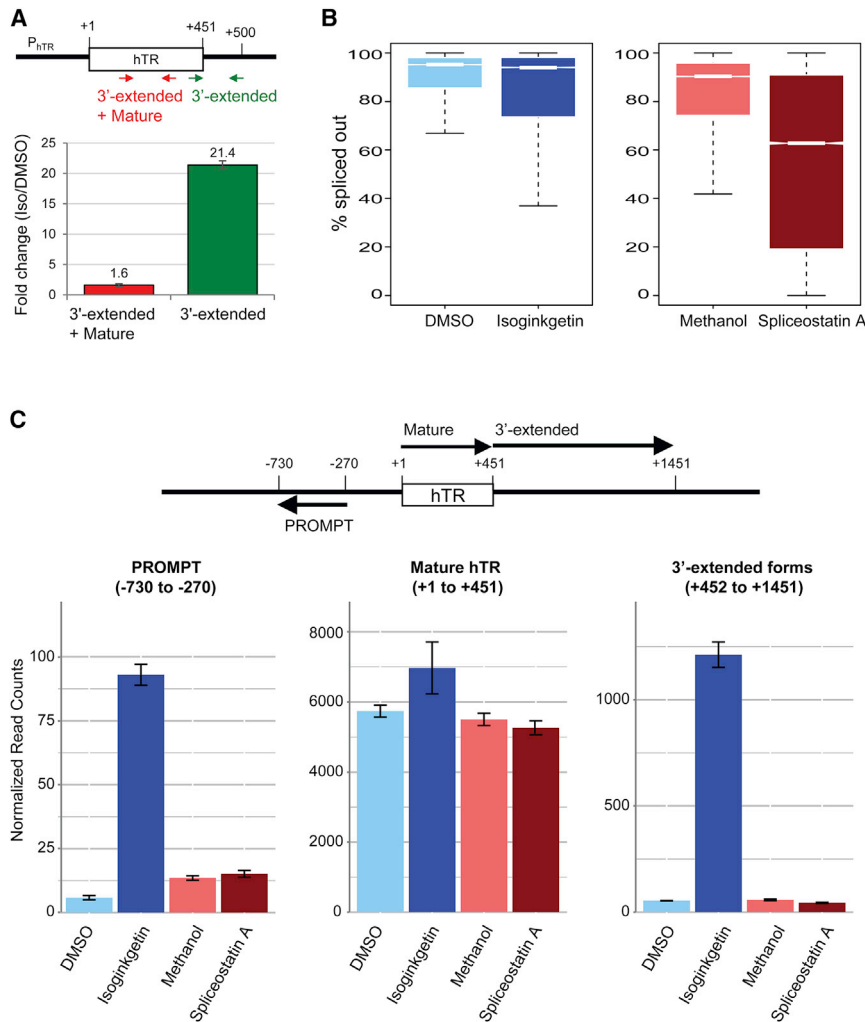


Figure 1. Isoginkgetin Mimics the Effects of Inhibiting the RNA Exosome

(A) HeLa S3 cells were treated with 35 μ M isoginkgetin or DMSO for 12 hr. Total RNA was prepared and subjected to qRT-PCR for *hTR*, *GAPDH*, *ATP5 β* , and *HPRT*. Positions of primers used to detect the mature and 3'-extended forms of hTR are indicated with arrows in the schematic. Bar graph of mean fold change for hTR relative to DMSO-treated samples and normalized to *GAPDH*, *ATP5 β* , and *HPRT*. Mean values were calculated from triplicate qRT-PCR experiments of three biological replicates, with bars representing SE.

(B) Splicing defect in HeLa S3 cells treated with 35 μ M isoginkgetin, DMSO, 200 nM spliceostatin A, or methanol for 12 hr. RNA-sequencing (RNA-seq) reads from ribo-depleted RNA were mapped using TopHat. Box plots were generated from the aggregate of 83,846 isoginkgetin and 85,427 (spliceostatin A) splicing units by calculating percent spliced out (PSO) values based on reads spanning the exon-exon junction relative to the sum of exon-intron, exon-exon, and intronic reads.

(C) Bar graphs showing quantification of RNA-seq reads mapping to genomic regions upstream (-730 to -270), within (+1 to +451), or downstream (+452 to +1,451) of hTR locus. The region of PROMPT, mature hTR, and 3'-extended hTR are indicated in the top schematic. All reads were normalized to library size. Mean values were calculated from three replicates, with bars representing SE.

Implication of NEXT and CBCA in the Turnover of 3' Extended Forms

The exosome is directed to its diverse RNA substrates and regulated in its activity by different adaptor and activator complexes (Mitchell, 2014). Two such complexes are prominent in the nucleus: the human homolog of the yeast Trf4/Air2/Mtr4 polyadenylation (TRAMP) complex and the nuclear exosome targeting (NEXT) complex. Human TRAMP is comprised of the Air2 homolog ZCCHC7, the non-canonical poly(A) polymerase TRF4-2/PAPD5 (Trf4 in yeast) and the MTR4 subunit, which is shared with NEXT. NEXT is composed of MTR4, ZCCHC8, and RBM7 (Lubas et al., 2011; Schilders et al., 2007). NEXT has been found to participate in the processing and elimination of a variety of RNAs, including PROMPTs, 3'-extended forms of snRNAs, and replication-dependent histone (RDH) transcripts (Andersen et al., 2013; Lubas et al., 2011), the same classes of RNAs we had seen increased upon isoginkgetin treatment.

Supporting a role for the NEXT complex in the turnover of hTR 3' extended forms, knockdown of ZCCHC8 and RBM7 (Figure 3A) increased the steady-state level of 3'-extended hTR (Figure 3B). In contrast, knockdown of the TRAMP-specific factor

ZCCHC7 had no effect, and TRF4-2 small interfering RNA (siRNA) treatment resulted in a small increase discussed further below. Most strikingly, knockdown of the shared component MTR4 caused a more than 12-fold increase in hTR 3' extended forms (Figure 3B). This may be explained by differences in knockdown efficiency, co-depletion of ZCCHC8 in the MTR4 knockdown (Figure 3A, left panel, lane 2), or cumulative effects of NEXT-dependent and -independent roles of MTR4 in hTR processing.

The cap binding complex A (CBCA) is composed of the cap-binding proteins 20 (CBP20) and 80 (CBP80) and arsenic-resistance protein 2 (ARS2). It binds the 7-methyl guanosine cap on nascent RNA pol II transcripts and, upon recruitment of ZC3H18 and NEXT, forms CBCA-NEXT, also known as CBCN (Andersen et al., 2013; Lubas et al., 2015). CBCN thereby links 5' capping to transcription termination and exosome-mediated 3' end processing or degradation (Figure 3C). Depletion of CBCN components causes increases in a subset of exosome substrates including PROMPTs and 3' extended forms of U1 and U2 snRNAs (Andersen et al., 2013). We found that depletion of CBP80 (Figure 3D) resulted in a close to 3-fold increase in the 3' extended forms of hTR, whereas siRNAs against ARS2 and ZC3H18 only caused small increases (Figure 3E). A more pronounced effect of CBP80 over ARS2 knockdown has also been observed in the context of pre-U2 accumulation (Andersen

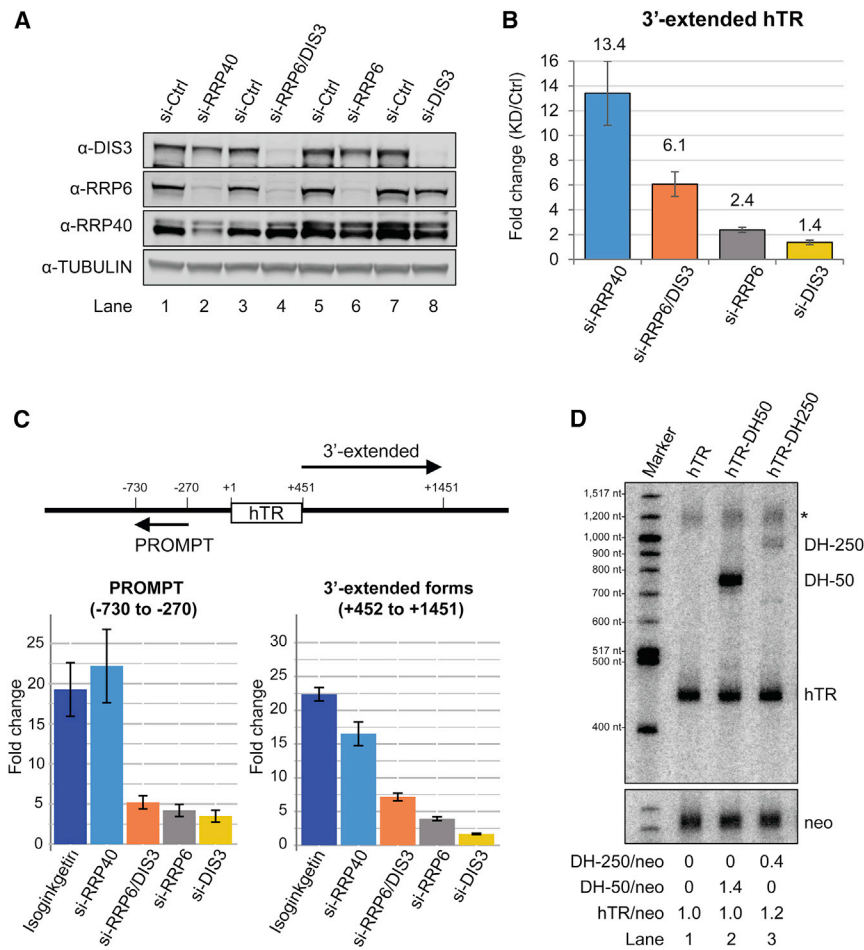


Figure 2. Longer Forms of hTR Are Preferentially Degraded

(A) Western blotting analysis of cell extracts prepared from HeLa cells treated with siRNAs targeting RRP40 (lane 2), RRP6 (lane 6), and DIS3 (lane 8), RRP6 (lane 6), and DIS3 (lane 8), respectively. Non-targeting siGENOME pool was used as control (lanes 1, 3, 5, and 7). Endogenous TUBULIN served as a loading control.

(B) Total RNA prepared from HeLa cells treated with the indicated siRNAs was subjected to qRT-PCR for 3'-extended hTR, GAPDH, ATP5β, and HPRT. Bar graph of mean fold change for 3'-extended hTR relative to control siRNA-treated samples and normalized to GAPDH, ATP5β, and HPRT. Mean values were calculated from triplicate qRT-PCR experiments of three biological replicates, with bars representing SE.

(C) Total RNA prepared from HeLa cells treated with 35 μM isoginkgetin or the indicated siRNAs was subjected to RNA-seq. RNA-seq reads mapping to genomic regions upstream (−730 to −270), within (+1 to +451), or downstream (+452 to +1,451) of hTR locus were normalized to library size. Y-axis represents the fold change in the indicated siRNA-treated samples relative to control siRNA or isoginkgetin-treated samples relative to DMSO control. Bars represent SE.

(D) pCR-XL-TOPO cloning vectors containing wild-type hTR or hTR harboring an additional double-hairpin structure of box H/ACA (fragments correspond to nucleotides ~206–451 of hTR) inserted 50 nt (double hairpin 50 nt downstream of hTR [DH-50], products corresponding to ~750 nt in length) or 250 nt (double hairpin 250 nt downstream of hTR [DH250], products corresponding to ~1,000 nt in length) downstream of the mature 3' end (position 451) were transfected into the telomerase-negative VA13 cells. Total RNA was prepared and subjected to northern blots. A probe against neomycin served as control for transfection efficiency and loading. An asterisk represents background resulted from pCR-XL-TOPO cloning vectors.

et al., 2013) and may reflect redundancy in factors connecting CBP20/80 with NEXT or a CBCA-independent role of CBC. Our results argue that the processing of 3'-extended hTR is mediated by CBC and NEXT and results primarily in degradation by the exosome. However, a fraction of transcripts must be processed into the mature form.

The Exosome, TRAMP, and CBC Function in hTR Processing

When hTR is examined by northern blotting, the dominant form appears as a distinct band. This form is generally referred to as the mature form, but the resolution afforded by 4% polyacrylamide gels does not permit distinction between the 451-nt mature RNA and slightly longer or shorter forms. Depletion of exosome components RRP40, RRP6, or RRP6/DIS3 caused an increase in this band (Figures 4A and S4). The effects were modest but highly reproducible over biological triplicates. Consistent with RRP6 being primarily responsible for the turnover of hTR, the ~451-nt RNA was increased by 1.4-fold upon

RRP6 knockdown but did not change upon DIS3 knockdown (Figure 4A).

Next, we examined the effects of TRAMP, NEXT, and CBCA knockdowns on hTR levels on northern blots. 2- to 3-fold increases were observed upon knockdown of MTR4 and CBP80, with smaller effects supporting roles for TRAMP and CBC in hTR turnover (Figure 4B). Knockdown of NEXT components ZCCHC8 and RBM7 had no effect. In aggregate, these data suggest that CBC, TRAMP, and the exosome are involved in the degradation of hTR forms that are ~451 nt in length, whereas NEXT plays a role in the degradation of longer transcripts.

To gain further insights into how the 451-nt mature form is produced, we performed RLM-RACE (RNA ligase-mediated rapid amplification of cDNA ends) coupled with high-throughput sequencing. In samples treated with control siRNA, ~75%–79% of hTR molecules matched the hTR sequence to position 451, ~4%–6% were truncated by up to 4 nt, and ~14%–18% extended beyond position 451 (Figure 4C). Consistent with an earlier report that examined hTR 3' ends (Goldfarb and Cech,

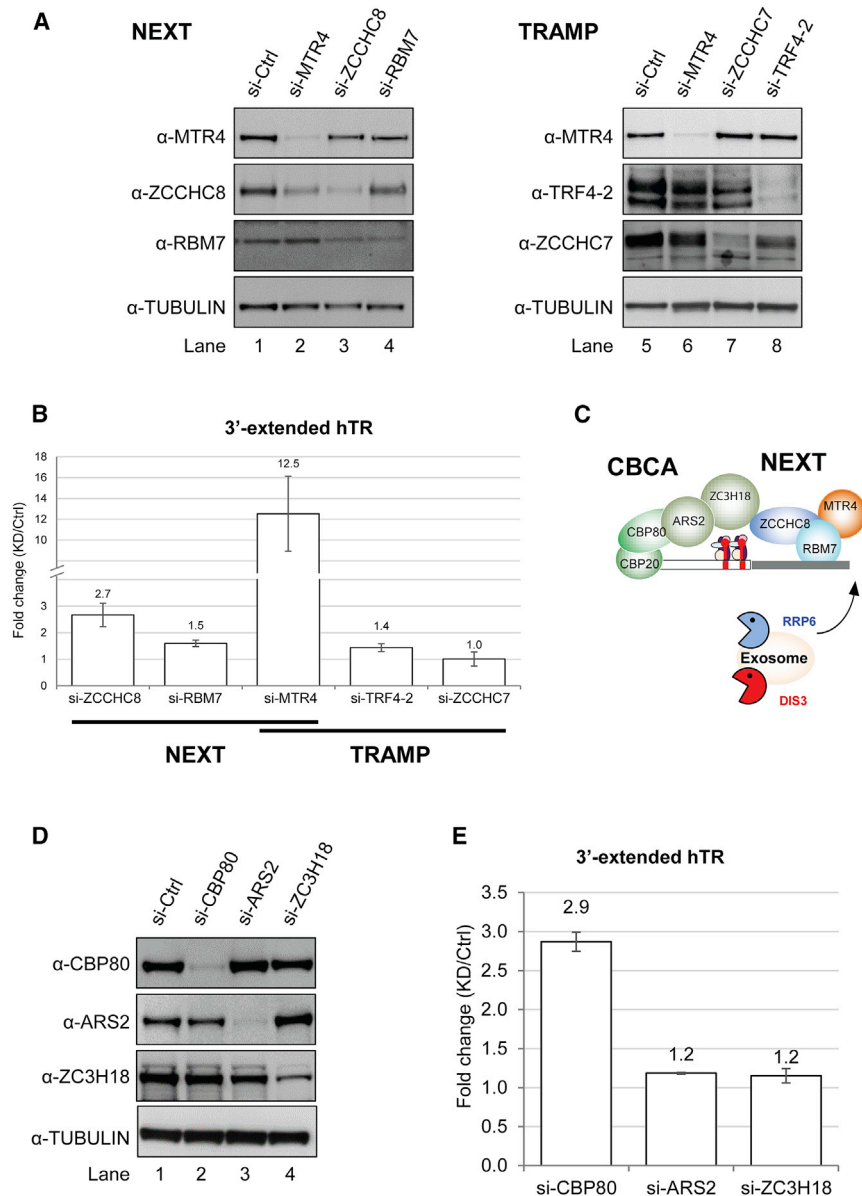


Figure 3. Implication of NEXT and CBCA in 3'-Extended hTR Turnover

(A) Western blotting analysis of cell lysates from HeLa cells treated with siRNAs against NEXT or TRAMP subunits. TUBULIN served as a loading control.

(B) Total RNA prepared from HeLa cells treated with the indicated siRNAs was subjected to qRT-PCR for 3'-extended *hTR*, *GAPDH*, *ATP5 β* , and *HPRT*. Mean fold change for 3'-extended hTR relative to control siRNA and normalized to multiple reference genes. Mean values were calculated from triplicate qRT-PCR experiments for each of two or three biological replicates. Bars represent SE.

(C) A schematic of exosome recruitment by CBCA and the NEXT complex.

(D) Western blot of cell lysates from HeLa cells treated with siRNAs against CBCA components. TUBULIN served as a loading control.

(E) qRT-PCR for 3' extended forms of hTR was performed as described in (B). Mean values were calculated from triplicate qRT-PCR experiments for each of two or three biological replicates, with bars representing SE.

2013), a fraction of molecules terminated in non-templated adenosines (Figure S5A). As the genome encodes for an adenosine at position 452, we cannot distinguish between mono-adenylated mature hTR and precursor terminating at position 452, but ~2% of hTR fell into this category (Figure S5A, shown in medium green). Knockdown of TRF4-2 reduced the oligo-adenylated fraction by 10-fold (Figure S5A, middle panel). A smaller decrease was observed following depletion of the TRAMP subunit ZCCHC7. This was not the case for the MTR4 knockdown, where oligo-adenylated forms increased, supporting the notion that TRF4-2 is responsible for oligo-adenylation of hTR with MTR4 playing a role downstream of oligo-adenylation in the degradation of hTR (Figure S5A).

Surprisingly, we found that knockdown of the exosome, CBCA, and ZC3H18 caused decreases in the fraction of

oligo-adenylated hTR (Figure S5A). Exosome depletion reduced oligo-adenylated hTR by 2- to 3-fold (Figure S5A, left). More dramatic effects were observed upon CBCA knockdown. Knockdown of CBP80 and ARS2 reduced the oligo-adenylated fraction by 5.8-fold and 10-fold, respectively and, like si-TRF4-2, increased the fraction of mature hTR (Figure S5A, right). A decrease in oligo-adenylated hTR caused by TRAMP and CBC knockdowns was further confirmed by oligo d(T)-primed qRT-PCR (Figure S5B). Consistent with observations of 3' sequencing analyses, oligo-adenylated hTR was decreased by 90% and 70% upon TRF4-2 and CBP80 knockdown, respectively. In addition to a reduction in oligo-adenylation, we also found that knockdown of the exosome, TRAMP, and CBCA reduced the fraction of hTR that is slightly longer than 451 nt, resulting in further increases in the mature form of hTR (Figure 4C, shown in light blue). Compared to the control (~14%–18%), the slightly longer form of hTR was reduced by knocking down the TRAMP components ZCCHC7 (5%) and TRF4-2 (3%) as well as the CBCA components CBP80 (2%), ARS2 (2%), and ZC3H18 (6%). Taken together, our data show that longer and oligo-adenylated forms of hTR are the precursor of the 451-nt mature RNA. Surprisingly, processing is attenuated in the presence of CBCA, TRAMP, and the exosome. This is inconsistent with a model in which the hTR precursor is processed by the CBCA/TRAMP/exosome complex. Instead, hTR maturation must be mediated by other nucleases

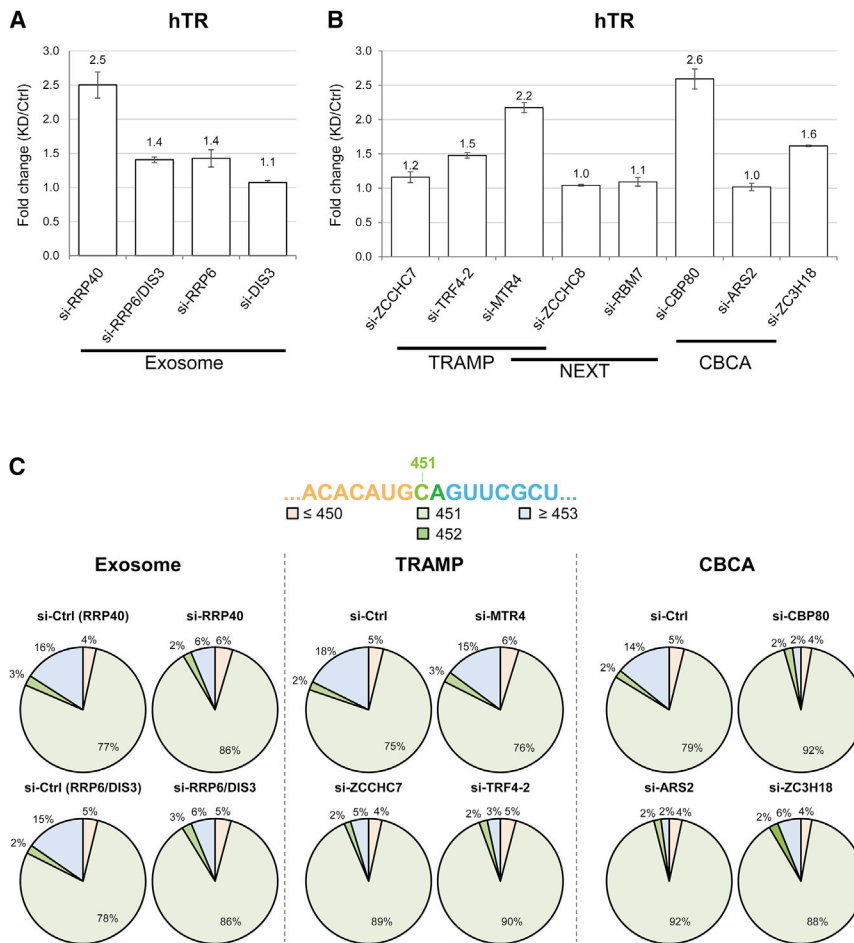


Figure 4. The Exosome, TRAMP, and CBC Function in hTR Processing

(A and B) Total RNA prepared from HeLa cells treated with the indicated siRNAs. Bar graph of mean fold change for hTR levels relative to control siRNA-treated samples and normalized to GAPDH RNA for the exosome (A), TRAMP and NEXT knockdown (B), and to 7SL RNA for CBCA knockdown (B). Mean values were calculated from northern blot experiments of three biological replicates. Bars represent SE.

(C) Pie chart illustrating distribution of the 3' end position. 3'-truncated (≤ 450), mature (451), and longer (≥ 453) forms of hTR are shown in light orange, green, and blue, respectively. Position 452 is shown in medium green. 3' ends were determined by RNA ligase-mediated 3' RACE approach. Number of reads analyzed: si-Ctrl (RRP40), 1412759; si-RRP40, 1412507; si-Ctrl (RRP6/DIS3), 1447919; si-RRP6/DIS3, 1485973; si-Ctrl (TRAMP), 1220990; si-MTR4, 1459392; si-ZCCHC7, 1333722; si-TRF4-2, 1281656; si-Ctrl (CBCA), 1072013; si-CBP80, 1346541; si-ARS2, 1501889; si-ZC3H18, 1353612.

that are in competition with degradation of the RNA by CBC, TRAMP, and the exosome (Figure S5C).

PARN Processes the 3' End of hTR

Our results suggest an unanticipated role for CBCA in inhibiting processing of hTR precursors by an activity that is in competition with the TRAMP/exosome complex (Figure 4). Three recent studies have implicated the poly(A)-specific ribonuclease PARN in telomere biology through the identification of mutations in patients with severe dyskeratosis congenita (Dhanraj et al., 2015; Stuart et al., 2015; Tummala et al., 2015). Although the reported reduction in hTR levels in patient samples could be an indirect consequence of reduced levels of dyskerin and other proteins involved in telomere biology (Tummala et al., 2015), an earlier report had implicated PARN in the processing of intron-encoded H/ACA box snoRNAs (Berndt et al., 2012). Interestingly, CBC has been shown to act as a negative regulator of PARN-mediated processing and CBP80 alone inhibits PARN activity in an m⁷G cap-independent manner (Balatsos et al., 2006). We therefore wondered whether PARN affected hTR biogenesis by processing the oligo-adenylated precursor of hTR. To examine the effect of PARN depletion on the extent of oligo-adenylation and steady-state level of precursor, we depleted PARN from HeLa cells (Figure 5A). PARN knockdown did not substantially

reduce the box H/ACA components at the protein level, although a shift of DKC1 to a faster-migrating form was observed (Figure 5A, lane 2). Oligo-adenylated hTR was increased by 5-fold upon PARN knockdown, as measured by oligo d(T)-primed qRT-PCR (Figure 5B). Sequencing of hTR 3' ends after RLM-RACE revealed that precursor was increased by 2-fold at the expense of

the 451-nt form (Figure 5C). These data support that PARN depletion results in deficiencies in the 3' end processing of hTR.

To further confirm the role of PARN in hTR 3' end processing, we overexpressed PARN in HeLa cells (Figure 5D). This did not significantly affect the steady-state level of hTR based on northern blots (Figure S6) but reduced oligo-adenylated hTR by over 30%, as measured by oligo d(T)-primed qRT-PCR (Figure 5E). 3' end sequence analysis revealed that the hTR precursor is reduced by 38% (Figure 5F), suggesting that PARN is involved in the deadenylation/3' end trimming of hTR.

Processing by PARN Is in Competition with Degradation

Knockdown of CBP80 and ARS2 greatly reduced the fractions of both precursor and oligo-adenylated forms of hTR (Figures 4 and S5), indicating that 3' end processing is more efficient in the absence of CBCA. If PARN is the enzyme that trims the 3' end of hTR precursor in the absence of PARN and CBP80, the hTR precursor should be stabilized in the absence of PARN and CBP80. We simultaneously knocked down PARN and CBP80 in HeLa cells (Figure 6A). Cells depleted of PARN and CBP80 indeed accumulated oligo-adenylated hTR (Figure 6B), supporting that CBP80 negatively regulates PARN activity.

Knockdown of CBC, TRAMP, and the exosome not only stabilized hTR levels but also facilitated the 3' end processing of hTR

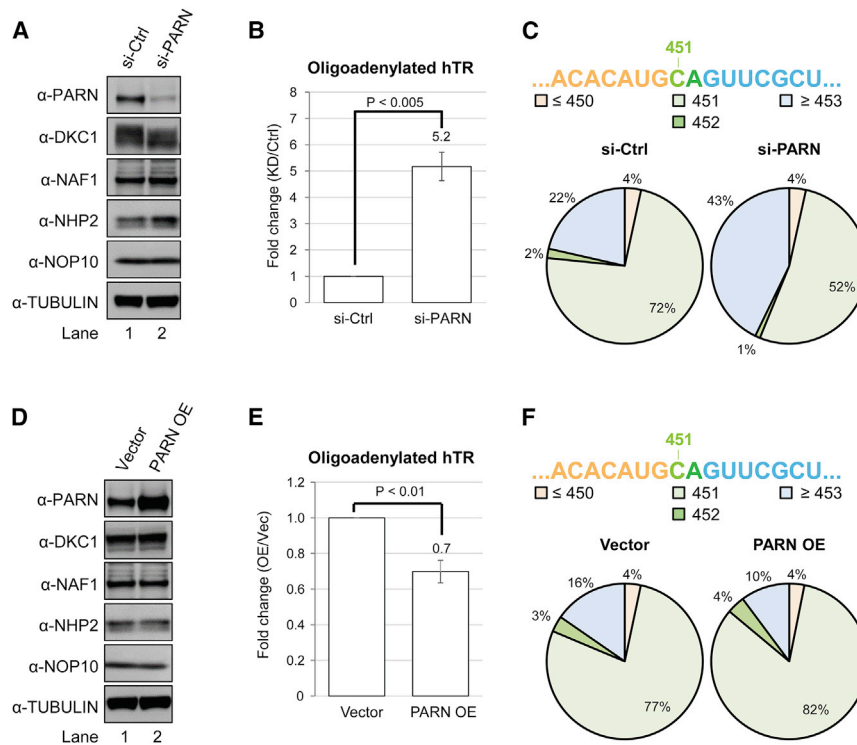


Figure 5. PARN Processes the 3' End of hTR

(A) Western blotting analysis of cell lysates from HeLa cells treated with siRNAs against PARN. Antibodies against PARN, dyskerin, NAF1, NHP2, and NOP10 were used. TUBULIN served as a loading control.

(B) Bar graph shows the mean fold change for oligo-adenylated hTR fraction relative to control siRNA and normalized to multiple reference genes. Oligo-adenylated hTR was measured by qRT-PCR using oligo dT primer for reverse transcription and cDNA amplification was done using hTR-specific primers. Mean fold changes were calculated from triplicate qRT-PCR experiments for each of three biological replicates, with bars representing SE.

(C) Pie chart illustrating distribution of the 3' end position. 3'-truncated (≤ 450), mature (451), and longer (≥ 453) forms of hTR are shown in light orange, green, and blue, respectively. Position 452 is shown in medium green. 3' ends were determined using an RNA ligase-mediated 3' RACE approach. Number of reads analyzed: si-Ctrl, 1761073; si-PARN, 1310308.

(D) Western blotting analysis of cell lysates from HeLa cells transfected with pCMV6-XL-PARN plasmid. Antibodies against PARN, dyskerin, NAF1, NHP2, and NOP10 were used. TUBULIN served as a loading control.

(E) Bar graph shows the mean fold change for oligo-adenylated hTR fraction relative to vector and normalized to multiple reference genes. Oligo-

adenylated hTR was measured as described in (B). Mean fold changes were calculated from triplicate qRT-PCR experiments for each of three biological replicates, with bars representing SE.

(F) Pie charts illustrating distribution of 3' end position as described in (C). Number of reads analyzed: vector, 1,223,760; PARN overexpression, 1,351,439.

precursors (Figure 4), indicating that degradation by CBC/TRAMP/exosome is in competition with PARN-mediated processing. We therefore wondered whether PARN deficiency affected the steady-state level of hTR. Knockdown of PARN in HeLa cells resulted in a 30% decrease in hTR by northern blots (Figure 6C, lane 2). Although we cannot rule out the possibility that reduced stability of hTR is an indirect effect, the observation that PARN knockdown caused a reduction in hTR fits the model that PARN functions in the precise trimming of hTR, a process that is in competition with degradation of these forms by the exosome aided by CBC and TRAMP. Consistent with this notion, simultaneous knockdown of PARN and any of several factors involved in the degradation of hTR rescued the mature form to wild-type levels (Figures 6C and 6D).

In aggregate, our data support a model in which long hTR transcripts are predominantly degraded by a pathway involving CBC, NEXT, and the exosome (Figure 7). A fraction of transcripts (hTR precursor) are oligo-adenylated, at least in part, by TRF4-2 and either degraded by the exosome or processed into mature form by PARN.

DISCUSSION

The exosome plays a central and evolutionarily conserved role in the processing, quality control, and degradation of many classes of RNAs (Houseley et al., 2006; Lykke-Andersen et al., 2009; Schneider and Tollervy, 2013). Here, we have shown that inhi-

bition of exosome activity by isoginkgetin or knockdown results in accumulation of long hTR transcripts that are normally degraded by the exosome in conjunction with CBCA and NEXT. Shorter precursors of hTR are oligo-adenylated in a process that depends on CBCA and TRAMP and are converted into mature hTR in a PARN-dependent manner. Maturation is therefore in competition with degradation by the exosome (Figure 7).

Diversity and Conservation in Telomerase RNA Processing

Substantial differences in TER biogenesis had been anticipated due to the fact that yeast telomerase RNAs share properties with snRNAs (Leonardi et al., 2008; Seto et al., 1999; Webb and Zakian, 2008), whereas mammalian telomerase RNA subunits resemble H/ACA box snoRNAs (Chen et al., 2000; Mitchell et al., 1999a). Even among yeasts, mechanisms for 3' end processing differ substantially. Whereas diverse yeasts and filamentous fungi rely on spliceosomal cleavage for 3' end processing of TER, *S. cerevisiae* TLC1 lacks an intron downstream of its mature 3' end, and transcriptional termination and processing involves the Nrd1-Nab3-Sen1 (NNS) pathway (Jamonak et al., 2011; Noël et al., 2012). Although human cells contain a homolog of Sen1, senataxin (Moreira et al., 2004), no homologs of Nrd1 or Nab3 have been identified, and there is presently no evidence supporting a role for senataxin in hTR biogenesis.

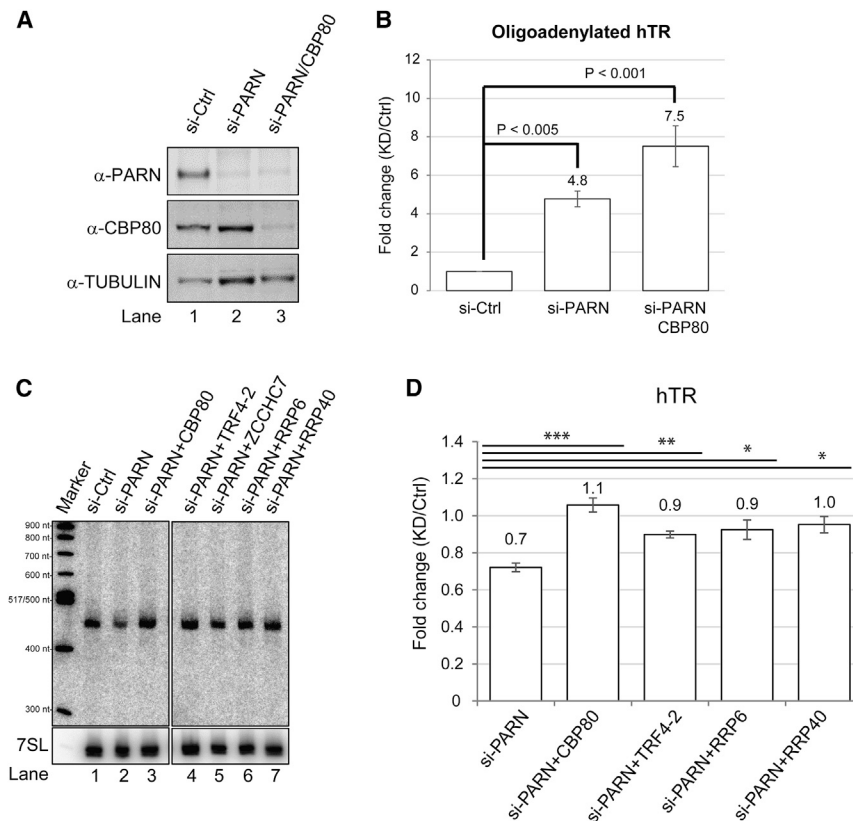


Figure 6. Processing by PARN Is in Competition with Degradation

(A) Western blotting analysis of cell lysates from HeLa cells treated with siRNAs against PARN and/or CBP80. TUBULIN served as a loading control.

(B) Bar graph shows the mean fold change for oligo-adenylated hTR fraction relative to control siRNA and normalized to multiple reference genes. Oligo-adenylated hTR was measured as described in Figure 5B. Mean fold changes were calculated from triplicate qRT-PCR experiments for each of three biological replicates, with bars representing SE.

(C) Northern blotting analysis of hTR from HeLa cells treated with siRNA against PARN alone or in combination with other factors as indicated. A probe against 7SL RNA served as a loading control.

(D) Bar graph shows the ratios of knockdown over control were normalized to 7SL RNA. Mean values were calculated from northern blot experiments of three biological replicates. Bars represent SE. Significance of change in hTR level between samples was calculated with a Student's t test; *p < 0.05, **p < 0.01, ***p < 0.005.

Accumulation of 3' extended forms of hTR upon knockdown of exosome, CBCA, or NEXT components supports a model in which CBC and the NEXT complex associate with hTR co-transcriptionally and recruit the exosome for 3' end processing and/or degradation. A similar connection was observed between the CBC and NNS complexes in *S. cerevisiae* (Vasiljeva and Buratowski, 2006), indicating that functional similarities may exist even though NNS and NEXT components are not related in sequence.

The association of the core exosome with two nucleases and cofactors with discrete properties and of distinct subcellular distribution are key features that provide specificity in the processing and degradation of different target RNAs. In human cells, spatial compartmentalization of different targeting complexes may further increase specificity of processing and degradation (Lubas et al., 2011). ZCCHC7 is strongly enriched in the nucleolus (Fasken et al., 2011; Lubas et al., 2011), suggesting that the TRAMP complex predominantly functions in this compartment. In contrast, RBM7 and ZCCHC8 are nucleoplasmic, consistent with a role for NEXT in recruiting the exosome to nascent transcripts (Lubas et al., 2011). While initial processing of 3'-extended hTR occurs co-transcriptionally in the nucleoplasm and is a prerequisite for translocation into the Cajal body (Theimer et al., 2007), degradation of mature hTR may occur in the nucleolus based on ZCCHC7 localization. The nucleolar exosome lacks DIS3 (Lubas et al., 2011), which could in part explain why depletion of DIS3, unlike RRP6, had no effect on mature hTR levels. However, current data do not exclude the possibility that a fraction of the longer forms escapes degradation and is processed into mature form.

et al., 2002), and humans (Marrone et al., 2004). In each system, reductions in the levels of telomerase RNA of as little as 30% to 50% result in telomere shortening. The effects of manipulating the activities of RNA processing factors reported here are therefore expected to have physiological consequences. Based on our data, the amount of mature hTR is determined in a kinetic competition between processing and degradation (Figure 7). The increase in all forms of hTR observed following MTR4, RRP40, or RRP6 knockdown indicates that a substantial fraction of hTR transcripts are normally degraded. The notion that precursor degradation limits hTR accumulation is also supported by the observation that insertion of a self-cleaving ribozyme immediately downstream of the mature 3' end resulted in increased accumulation of mature form (Egan and Collins, 2012b).

The broad association of human CBC with the 5' ends of pol II transcripts and the promiscuous binding of RBM7 to U-rich sequences on nascent RNA creates a surveillance mechanism to target the exosome to unprotected 3' ends (Andersen et al., 2013; Lubas et al., 2015). PROMPTs and extended transcripts of replication-dependent histones and snRNAs are transcriptionally terminated and subsequently degraded in this manner. The accumulation of 3' extended forms of hTR upon knockdown of CBC or NEXT components indicates that hTR transcripts enter the same pathway. What is less clear is whether CBCN-mediated termination necessarily leads to degradation of 3' extended hTR or whether degradation turns into processing for a fraction of transcripts. This decision is likely affected by how rapidly

degradation by the exosome. The balance between those fates determines the amount of mature hTR that is produced.

In summary, these results show that processing and degradation of hTR precursors are in kinetic competition and favoring one process over another shifts the balance to generate more or less mature form. This establishes a framework for how mature hTR is generated from longer transcripts and how subtle shifts in the balance between competing pathways affects the amount of functional telomerase RNA that is ultimately produced. A clear understanding of the mechanisms involved in hTR maturation and turnover holds promise for medical intervention in cases where a mutation in a processing factor shifts the balance toward degradation, resulting in a lower steady-state level of hTR, insufficient telomerase activity, and premature telomere shortening. The finding that most of the hTR transcripts are normally degraded is encouraging in that attenuation of degradation may be used to boost the level of functional telomerase RNA in patients with telomerase insufficiency syndromes caused by low levels of hTR.

EXPERIMENTAL PROCEDURES

Cell Culture and RNAi Analysis

HeLa cells were cultured in DMEM (Life Technologies, 11995-065) containing 10% fetal bovine serum (Sigma-Aldrich) at 37°C, 5% CO₂. VA13 cells (WI38 VA13 subline 2RA purchased from American Type Culture Collection [ATCC]) were cultured in ATCC formulated Eagle's minimum essential medium (ATCC 30-2003) with 10% fetal bovine serum (Sigma) at 37°C, 5% CO₂. Sequences of siRNAs are listed in Table S1. For isoginkgetin and spliceostatin A treatment, isoginkgetin was purchased from EMD Millipore Chemicals (vendor part #CAS548-19-6). Spliceostatin A was a gift from Dr. Minoru Yoshida. HeLa S3 cells were treated with 35 μM isoginkgetin and 200 nM spliceostatin A, respectively, for 12 hr. Control cells were treated with DMSO (0.1% v/v) for isoginkgetin and methanol (0.1% v/v) for spliceostatin A. For siRNA knockdown, cells were treated twice (2- or 3-day interval) with 20 nM or 40 nM siRNA using Dharmafect I (Dharmacon). For PARN overexpression, PARN-pCMV6-XL (Origene, SC325208) was transfected into HeLa cells using Fugene HD (Promega) for 72 hr. For western blotting analysis, cells were lysed in a solution containing 2× LDS sampling buffer (Life Technologies), 0.78% β-mercaptoethanol (v/v) (J.T. Baker), and 4% SDS. Antibodies used for western blotting are listed in Table S2.

qRT-PCR

Cells were washed once with Dulbecco's PBS and collected in Trizol reagent (Ambion, Life Technologies) according to the manufacturer's instructions, followed by treatment with DNase I (New England Biolabs) at 37°C for 30 min. RNA was extracted with phenol/chloroform equilibrated with 50 mM NaOAc (pH 5.0) and ethanol precipitated. RNA was used for qRT-PCR and northern blotting analyses. Reverse-transcription reactions (20 μl) containing 2 μg RNA, 1× Vilo reaction mix (Life Technologies, 11754-250), and 1× Superscript III enzyme blend (Life Technologies, 11754-250) were incubated at 25°C for 10 min, 42°C for 1 hr, and 85°C for 5 min in a PCR machine. Reactions were then diluted 25-fold with water. Forward and reverse primers used for qPCR are listed in Table S3. The diluted cDNA and pre-mix components (1× Perfecta SYBR green fastmix ROX, 625 nM forward and reverse primers) were mixed in a 384-well microplate by a CAS4200 robot, and qPCR reactions were performed in triplicates in a 7900 HT Fast Real-Time PCR system. All data were normalized to multiple reference genes (GAPDH, ATP5β, and HPRT) by Biogazelle's qbase+ software.

Northern Blot

For northern analysis of hTR, 10 μg total RNA was used. RNA was separated on a 4% polyacrylamide (29:1) gel containing 8 M urea and transferred to

Hybond-N1 nylon membrane (GE Healthcare) at 400 mA for 1 hr in 0.5× TBE buffer. RNA was cross-linked to the membrane in a Stratalinker (Stratagene; 254 nm, 120 mJ). Hybridizations with radiolabeled probes were performed in Church-Gilbert buffer at 65°C (hTR, and GAPDH probes generated by nick-translation of a PCR fragment in the presence of ³²P-α-dCTP) or 42°C for the oligonucleotide probe against 7SL (BLoli5349) and neomycin (BLoli2948). Oligonucleotides used for preparation of probes are listed in Table S4 and were labeled with T4 polynucleotide kinase in the presence of ³²P-γ-ATP.

RNA-Ligase-Mediated 3' RACE with Deep Sequencing

Library preparation was based on a published protocol (Goldfarb and Cech, 2013). Oligonucleotides used for library preparation are listed in Table S5. Ligation reactions contained 1.5 μg DNase I-treated total RNA, 3.7% PEG8000, 7.4% DMSO, 1× T4 RNA ligase buffer, 10 U T4 RNA ligase I, 0.7 mM ATP, and 3.7 μM 3' linker (BLoli5511, IDT miRNA linker 3). The ligation reaction was incubated at 16°C for 18 hr and inactivated at 65°C for 15 min. RNA ligation reactions were annealed with 1.6 μM RT primer (BLoli5575) and 0.5 μM dNTPs at 65°C for 5 min, cooled down to room temperature for 10 min, and transferred to 55°C for reverse transcription in 30 μl volumes containing 1× First Strand buffer, 5 mM DTT, 40 U RNasin plus RNase inhibitor (Promega), and 300 U Superscript III (Invitrogen) for 60 min. 10 U RNase H was added into the reverse transcription reaction, followed by incubation at 37°C for 20 min and heat-inactivation at 70°C for 15 min. The first round PCR was performed with 0.5 μM BLoli5575 and BLoli5574 in 50 μl volumes containing 1× Phusion HF buffer, 0.2 mM dNTPs, 1 U Phusion Hot Start II polymerase (Thermo Scientific) using the following program: 98°C for 30 s, 15 cycles of 98°C for 30 s, 57°C for 30 s, 72°C for 30 s, and final extension at 72°C for 10 min. First-round PCR products were purified by PCR purification kit (QIAGEN). Then, 5 μl of 10×-diluted first-round PCR product was used as template for the second round PCR reactions containing 0.5 μM BLoli4666 and respective indexed primers as indicated in Table S5, 1× Phusion HF buffer, 0.2 mM dNTPs, and 1 U Phusion Hot Start II polymerase with the following program: 98°C for 30 s, 15 cycles of 98°C for 30 s, 57°C for 30 s, 72°C for 30 s, and final extension at 72°C for 10 min. Amplicons were purified by PCR purification kit (QIAGEN) and the primer dimers were removed using the Pippin Prep System (Sage Science), then quantified by Qubit and Bioanalyzer. The samples were sequenced on the Illumina HiSeq using RapidSeq 100-bp single-end reads. The samples were multiplexed and split between two lanes. There are 2.1 to 13.6 million reads per sample after filtering for quality. Reads were binned into the various forms of hTR using custom python scripts, and the number of reads in each bin was normalized to library size.

ACCESSION NUMBERS

The accession numbers for the data sets reported in this paper are GEO: GSE72055 and GEO: GSE73776.

SUPPLEMENTAL INFORMATION

Supplemental Information includes Supplemental Experimental Procedures, six figures, and five tables and can be found with this article online at <http://dx.doi.org/10.1016/j.celrep.2015.10.075>.

AUTHOR CONTRIBUTIONS

C.-K.T. and P.B. designed the experiments; C.-K.T. performed most of the experiments; H.-F.W. carried out knockdown experiments and protein and RNA isolation and performed qRT-PCR for hTR. C.-K.T. and H.-F.W. generated northern blots and performed 3' end analysis of hTR. A.M.B. produced and analyzed RNA-seq data, carried out the experiments with splicing inhibitors, and generated most of the western blots; C.-K.T. performed RLM-RACE experiments, and M.R.S. analyzed the Illumina data. M.G. carried out the initial characterization of the effects of splicing inhibitors and generated and tested

the double H/ACA constructs. All authors analyzed the data, and C.-K.T. and P.B. wrote the manuscript.

ACKNOWLEDGMENTS

We thank Minoru Yoshida for the gift of spliceostatin A, Francois Bachand for communicating data prior to publication, Wuxiang Guan for early contributions to this project, and other members of the Baumann laboratory for discussions. This work was funded in part by the Stowers Institute for Medical Research. P.B. is an Investigator with the Howard Hughes Medical Institute. Original data underlying this manuscript can be accessed from the Stowers Original Data Repository at <http://www.stowers.org/pubs/LIBPB-807>.

Received: June 4, 2015

Revised: October 2, 2015

Accepted: October 27, 2015

Published: November 25, 2015

REFERENCES

- Andersen, P.R., Domanski, M., Kristiansen, M.S., Storvall, H., Ntini, E., Verheggen, C., Schein, A., Bunkenborg, J., Poser, I., Hallais, M., et al. (2013). The human cap-binding complex is functionally connected to the nuclear RNA exosome. *Nat. Struct. Mol. Biol.* *20*, 1367–1376.
- Armanios, M.Y., Chen, J.J., Cogan, J.D., Alder, J.K., Ingersoll, R.G., Markin, C., Lawson, W.E., Xie, M., Vulto, I., Phillips, J.A., 3rd., et al. (2007). Telomerase mutations in families with idiopathic pulmonary fibrosis. *N. Engl. J. Med.* *356*, 1317–1326.
- Balatsos, N.A., Nilsson, P., Mazza, C., Cusack, S., and Virtanen, A. (2006). Inhibition of mRNA deadenylation by the nuclear cap binding complex (CBC). *J. Biol. Chem.* *281*, 4517–4522.
- Berndt, H., Harnisch, C., Rammelt, C., Stöhr, N., Zirkel, A., Dohm, J.C., Himmelbauer, H., Tavanez, J.P., Hüttelmaier, S., and Wahle, E. (2012). Maturation of mammalian H/ACA box snoRNAs: PAPD5-dependent adenylation and PARN-dependent trimming. *RNA* *18*, 958–972.
- Boulon, S., Marmier-Gourrier, N., Pradet-Balade, B., Wurth, L., Verheggen, C., Jány, B.E., Rothé, B., Pescia, C., Robert, M.C., Kiss, T., et al. (2008). The Hsp90 chaperone controls the biogenesis of L7Ae RNP through conserved machinery. *J. Cell Biol.* *180*, 579–595.
- Box, J.A., Bunch, J.T., Tang, W., and Baumann, P. (2008). Spliceosomal cleavage generates the 3' end of telomerase RNA. *Nature* *456*, 910–914.
- Chen, J.L., Blasco, M.A., and Greider, C.W. (2000). Secondary structure of vertebrate telomerase RNA. *Cell* *100*, 503–514.
- Coy, S., Volanakis, A., Shah, S., and Vasiljeva, L. (2013). The Sm complex is required for the processing of non-coding RNAs by the exosome. *PLoS ONE* *8*, e65606.
- Dhanraj, S., Gunja, S.M., Deveau, A.P., Nissbeck, M., Boonyawat, B., Coombs, A.J., Renieri, A., Mucciolo, M., Marozza, A., Buoni, S., et al. (2015). Bone marrow failure and developmental delay caused by mutations in poly(A)-specific ribonuclease (PARN). *J. Med. Genet.* *52*, 738–748.
- Egan, E.D., and Collins, K. (2012a). Biogenesis of telomerase ribonucleoproteins. *RNA* *18*, 1747–1759.
- Egan, E.D., and Collins, K. (2012b). An enhanced H/ACA RNP assembly mechanism for human telomerase RNA. *Mol. Cell Biol.* *32*, 2428–2439.
- Fasken, M.B., Leung, S.W., Banerjee, A., Kodani, M.O., Chavez, R., Bowman, E.A., Purohit, M.K., Rubinson, M.E., Rubinson, E.H., and Corbett, A.H. (2011). Air1 zinc knuckles 4 and 5 and a conserved IWRXY motif are critical for the function and integrity of the Trf4/5-Air1/2-Mtr4 polyadenylation (TRAMP) RNA quality control complex. *J. Biol. Chem.* *286*, 37429–37445.
- Feng, J., Funk, W.D., Wang, S.S., Weinrich, S.L., Avilion, A.A., Chiu, C.P., Adams, R.R., Chang, E., Allsopp, R.C., Yu, J., et al. (1995). The RNA component of human telomerase. *Science* *269*, 1236–1241.
- Fu, D., and Collins, K. (2003). Distinct biogenesis pathways for human telomerase RNA and H/ACA small nucleolar RNAs. *Mol. Cell* *11*, 1361–1372.
- Fu, D., and Collins, K. (2007). Purification of human telomerase complexes identifies factors involved in telomerase biogenesis and telomere length regulation. *Mol. Cell* *28*, 773–785.
- Goldfarb, K.C., and Cech, T.R. (2013). 3' terminal diversity of MRP RNA and other human noncoding RNAs revealed by deep sequencing. *BMC Mol. Biol.* *14*, 23.
- Grozdanov, P.N., Roy, S., Kittur, N., and Meier, U.T. (2009). SHQ1 is required prior to NAF1 for assembly of H/ACA small nucleolar and telomerase RNPs. *RNA* *15*, 1188–1197.
- Gunisova, S., Elboher, E., Nosek, J., Gorkovoy, V., Brown, Y., Lucier, J.F., Latereur, N., Wellinger, R.J., Tzfati, Y., and Tomaska, L. (2009). Identification and comparative analysis of telomerase RNAs from *Candida* species reveal conservation of functional elements. *RNA* *15*, 546–559.
- Hathcock, K.S., Hemann, M.T., Opperman, K.K., Strong, M.A., Greider, C.W., and Hodes, R.J. (2002). Haploinsufficiency of mTR results in defects in telomere elongation. *Proc. Natl. Acad. Sci. USA* *99*, 3591–3596.
- Hoareau-Aveilla, C., Bonoli, M., Caizergues-Ferrer, M., and Henry, Y. (2006). hNaf1 is required for accumulation of human box H/ACA snoRNPs, scaRNPs, and telomerase. *RNA* *12*, 832–840.
- Houseley, J., LaCava, J., and Tollervy, D. (2006). RNA-quality control by the exosome. *Nat. Rev. Mol. Cell Biol.* *7*, 529–539.
- Jamonnak, N., Creamer, T.J., Darby, M.M., Schaughency, P., Wheelan, S.J., and Corden, J.L. (2011). Yeast Nrd1, Nab3, and Sen1 transcriptome-wide binding maps suggest multiple roles in post-transcriptional RNA processing. *RNA* *17*, 2011–2025.
- Kaida, D., Motoyoshi, H., Tashiro, E., Nojima, T., Hagiwara, M., Ishigami, K., Watanabe, H., Kitahara, T., Yoshida, T., Nakajima, H., et al. (2007). Spliceostatin A targets SF3b and inhibits both splicing and nuclear retention of pre-mRNA. *Nat. Chem. Biol.* *3*, 576–583.
- Kannan, R., Hartnett, S., Voelker, R.B., Berglund, J.A., Staley, J.P., and Baumann, P. (2013). Intronic sequence elements impede exon ligation and trigger a discard pathway that yields functional telomerase RNA in fission yeast. *Genes Dev.* *27*, 627–638.
- Kannan, R., Helston, R.M., Dannebaum, R.O., and Baumann, P. (2015). Diverse mechanisms for spliceosome-mediated 3' end processing of telomerase RNA. *Nat. Commun.* *6*, 6104.
- Kiss, T., Fayet, E., Jány, B.E., Richard, P., and Weber, M. (2006). Biogenesis and intranuclear trafficking of human box C/D and H/ACA RNPs. *Cold Spring Harb. Symp. Quant. Biol.* *71*, 407–417.
- Kiss, T., Fayet-Lebaron, E., and Jány, B.E. (2010). Box H/ACA small ribonucleoproteins. *Mol. Cell* *37*, 597–606.
- Kuehner, J.N., Pearson, E.L., and Moore, C. (2011). Unravelling the means to an end: RNA polymerase II transcription termination. *Nat. Rev. Mol. Cell Biol.* *12*, 283–294.
- Kuprys, P.V., Davis, S.M., Hauer, T.M., Meltzer, M., Tzfati, Y., and Kirk, K.E. (2013). Identification of telomerase RNAs from filamentous fungi reveals conservation with vertebrates and yeasts. *PLoS ONE* *8*, e58661.
- Leonardi, J., Box, J.A., Bunch, J.T., and Baumann, P. (2008). TER1, the RNA subunit of fission yeast telomerase. *Nat. Struct. Mol. Biol.* *15*, 26–33.
- Lubas, M., Christensen, M.S., Kristiansen, M.S., Domanski, M., Falkenby, L.G., Lykke-Andersen, S., Andersen, J.S., Dziembowski, A., and Jensen, T.H. (2011). Interaction profiling identifies the human nuclear exosome targeting complex. *Mol. Cell* *43*, 624–637.
- Lubas, M., Andersen, P.R., Schein, A., Dziembowski, A., Kudla, G., and Jensen, T.H. (2015). The human nuclear exosome targeting complex is loaded onto newly synthesized RNA to direct early ribonucleolysis. *Cell Rep.* *10*, 178–192.
- Lykke-Andersen, S., Brodersen, D.E., and Jensen, T.H. (2009). Origins and activities of the eukaryotic exosome. *J. Cell Sci.* *122*, 1487–1494.
- Marrone, A., Stevens, D., Vulliamy, T., Dokal, I., and Mason, P.J. (2004). Heterozygous telomerase RNA mutations found in dyskeratosis congenita and aplastic anemia reduce telomerase activity via haploinsufficiency. *Blood* *104*, 3936–3942.

- Mayas, R.M., Maita, H., and Staley, J.P. (2006). Exon ligation is proofread by the DExD/H-box ATPase Prp22p. *Nat. Struct. Mol. Biol.* **13**, 482–490.
- Mitchell, P. (2014). Exosome substrate targeting: the long and short of it. *Biochem. Soc. Trans.* **42**, 1129–1134.
- Mitchell, J.R., Cheng, J., and Collins, K. (1999a). A box H/ACA small nucleolar RNA-like domain at the human telomerase RNA 3' end. *Mol. Cell. Biol.* **19**, 567–576.
- Mitchell, J.R., Wood, E., and Collins, K. (1999b). A telomerase component is defective in the human disease dyskeratosis congenita. *Nature* **402**, 551–555.
- Moreira, M.C., Klur, S., Watanabe, M., Németh, A.H., Le Ber, I., Moniz, J.C., Tranchant, C., Aubourg, P., Tazir, M., Schöls, L., et al. (2004). Senataxin, the ortholog of a yeast RNA helicase, is mutant in ataxia-ocular apraxia 2. *Nat. Genet.* **36**, 225–227.
- Mozdy, A.D., and Cech, T.R. (2006). Low abundance of telomerase in yeast: implications for telomerase haploinsufficiency. *RNA* **12**, 1721–1737.
- Nandakumar, J., and Cech, T.R. (2013). Finding the end: recruitment of telomerase to telomeres. *Nat. Rev. Mol. Cell Biol.* **14**, 69–82.
- Nguyen, D., St-Sauveur, V.G., Bergeron, D., Dupuis-Sandoval, F., Scott, M.S., and Bachand, F. (2015). A polyadenylation-dependent 3' end maturation pathway is required for the synthesis of the human telomerase RNA. *Cell Rep.* **13**, Published online November 25, 2015. <http://dx.doi.org/10.1016/j.celrep.2015.11.003>.
- Noël, J.F., Larose, S., Abou Elela, S., and Wellinger, R.J. (2012). Budding yeast telomerase RNA transcription termination is dictated by the Nrd1/Nab3 non-coding RNA termination pathway. *Nucleic Acids Res.* **40**, 5625–5636.
- O'Brien, K., Matlin, A.J., Lowell, A.M., and Moore, M.J. (2008). The biflavonoid isoginkgetin is a general inhibitor of Pre-mRNA splicing. *J. Biol. Chem.* **283**, 33147–33154.
- Podlevsky, J.D., Bley, C.J., Omana, R.V., Qi, X., and Chen, J.J. (2008). The telomerase database. *Nucleic Acids Res.* **36**, D339–D343.
- Preker, P., Nielsen, J., Kammler, S., Lykke-Andersen, S., Christensen, M.S., Mapendano, C.K., Schierup, M.H., and Jensen, T.H. (2008). RNA exosome depletion reveals transcription upstream of active human promoters. *Science* **322**, 1851–1854.
- Qi, X., Rand, D.P., Podlevsky, J.D., Li, Y., Mosig, A., Stadler, P.F., and Chen, J.J. (2015). Prevalent and distinct spliceosomal 3'-end processing mechanisms for fungal telomerase RNA. *Nat. Commun.* **6**, 6105.
- Schilders, G., van Dijk, E., and Pruijn, G.J. (2007). C1D and hMtr4p associate with the human exosome subunit PM/Scf-100 and are involved in pre-rRNA processing. *Nucleic Acids Res.* **35**, 2564–2572.
- Schneider, C., and Tollervey, D. (2013). Threading the barrel of the RNA exosome. *Trends Biochem. Sci.* **38**, 485–493.
- Seto, A.G., Zaug, A.J., Sobel, S.G., Wolin, S.L., and Cech, T.R. (1999). *Saccharomyces cerevisiae* telomerase is an Sm small nuclear ribonucleoprotein particle. *Nature* **401**, 177–180.
- Shukla, S., and Parker, R. (2014). Quality control of assembly-defective U1 snRNAs by decapping and 5'-to-3' exonucleolytic digestion. *Proc. Natl. Acad. Sci. USA* **111**, E3277–E3286.
- Stewart, S.A., and Weinberg, R.A. (2006). Telomeres: cancer to human aging. *Annu. Rev. Cell Dev. Biol.* **22**, 531–557.
- Stuart, B.D., Choi, J., Zaidi, S., Xing, C., Holohan, B., Chen, R., Choi, M., Dharmwadkar, P., Torres, F., Girod, C.E., et al. (2015). Exome sequencing links mutations in PARN and RTEL1 with familial pulmonary fibrosis and telomere shortening. *Nat. Genet.* **47**, 512–517.
- Theimer, C.A., Jády, B.E., Chim, N., Richard, P., Breece, K.E., Kiss, T., and Feigon, J. (2007). Structural and functional characterization of human telomerase RNA processing and cajal body localization signals. *Mol. Cell* **27**, 869–881.
- Tudek, A., Porrua, O., Kabzinski, T., Lidschreiber, M., Kubicek, K., Fortova, A., Lacroute, F., Vanacova, S., Cramer, P., Stefl, R., and Libri, D. (2014). Molecular basis for coordinating transcription termination with noncoding RNA degradation. *Mol. Cell* **55**, 467–481.
- Tummala, H., Walne, A., Collopy, L., Cardoso, S., de la Fuente, J., Lawson, S., Powell, J., Cooper, N., Foster, A., Mohammed, S., et al. (2015). Poly(A)-specific ribonuclease deficiency impacts telomere biology and causes dyskeratosis congenita. *J. Clin. Invest.* **125**, 2151–2160.
- Vasiljeva, L., and Buratowski, S. (2006). Nrd1 interacts with the nuclear exosome for 3' processing of RNA polymerase II transcripts. *Mol. Cell* **21**, 239–248.
- Venteicher, A.S., Meng, Z., Mason, P.J., Veenstra, T.D., and Artandi, S.E. (2008). Identification of ATPases pontin and reptin as telomerase components essential for holoenzyme assembly. *Cell* **132**, 945–957.
- Vulliamy, T., Marrone, A., Goldman, F., Dearlove, A., Bessler, M., Mason, P.J., and Dokal, I. (2001). The RNA component of telomerase is mutated in autosomal dominant dyskeratosis congenita. *Nature* **413**, 432–435.
- Vulliamy, T., Marrone, A., Dokal, I., and Mason, P.J. (2002). Association between aplastic anaemia and mutations in telomerase RNA. *Lancet* **359**, 2168–2170.
- Webb, C.J., and Zakian, V.A. (2008). Identification and characterization of the *Schizosaccharomyces pombe* TER1 telomerase RNA. *Nat. Struct. Mol. Biol.* **15**, 34–42.
- Yi, X., Tesmer, V.M., Savre-Train, I., Shay, J.W., and Wright, W.E. (1999). Both transcriptional and posttranscriptional mechanisms regulate human telomerase template RNA levels. *Mol. Cell. Biol.* **19**, 3989–3997.
- Zhu, Y., Qi, C., Cao, W.Q., Yeldandi, A.V., Rao, M.S., and Reddy, J.K. (2001). Cloning and characterization of PIMT, a protein with a methyltransferase domain, which interacts with and enhances nuclear receptor coactivator PRIP function. *Proc. Natl. Acad. Sci. USA* **98**, 10380–10385.